

# Deformed shell model results for neutrinoless double beta decay of nuclei in A=60-90 region

R. Sahu<sup>1\*</sup> and V.K.B. Kota<sup>2,3</sup>

<sup>1</sup>*Physics Department, Berhampur University,  
Berhampur-760 007, Odisha, INDIA and*

<sup>2</sup>*Physical Research Laboratory, Ahmedabad - 380 009, INDIA*

<sup>3</sup>*Department of Physics, Laurentian University,  
Sudbury, ON P3E 2C6, CANADA*

## Abstract

Nuclear transition matrix elements (NTME) for the neutrinoless double beta decay of  $^{70}\text{Zn}$ ,  $^{80}\text{Se}$  and  $^{82}\text{Se}$  nuclei are calculated within the framework of the deformed shell model based on Hartree-Fock states. For  $^{70}\text{Zn}$ , jj44b interaction in  $^2p_{3/2}$ ,  $^1f_{5/2}$ ,  $^2p_{1/2}$  and  $^1g_{9/2}$  space with  $^{56}\text{Ni}$  as the core is employed. However, for  $^{80}\text{Se}$  and  $^{82}\text{Se}$  nuclei, a modified Kuo interaction with the above core and model space are employed. Most of our calculations in this region were performed with this effective interaction. However, jj44b interaction has been found to be better for  $^{70}\text{Zn}$ . The above model space was used in many recent shell model and interacting boson model calculations for nuclei in this region. After ensuring that DSM gives good description of the spectroscopic properties of low-lying levels in these three nuclei considered, the NTME are calculated. The deduced half-lives with these NTME, assuming neutrino mass is 1 eV, are  $1.1 \times 10^{26}$  yr,  $2.3 \times 10^{27}$  yr and  $2.2 \times 10^{24}$  yr for  $^{70}\text{Zn}$ ,  $^{80}\text{Se}$  and  $^{82}\text{Se}$ , respectively.

PACS numbers: 23.40.Hc, 21.10.Tg, 21.60.Jz, 27.50.+e

---

\*Electronic address: rankasahu@rediffmail.com

## I. INTRODUCTION

Neutrinoless double beta decay ( $0\nu\beta\beta$  or  $0\nu DBD$ ) which involves emission of two electrons without the accompanying neutrinos and which violates lepton number conservation has been an important and challenging problem both for the experimentalists and theoreticians. Recent neutrino oscillation experiments have demonstrated that neutrinos have mass. The observation of  $0\nu\beta\beta$  decay is expected to provide information regarding the absolute neutrino mass which is not known. To extract neutrino mass, the nuclear matrix elements must be known from a reliable nuclear model and hence the main goal of nuclear theorists is to calculate the nuclear transition matrix elements as accurately as possible. On the other hand experimental programmes have been initiated at different laboratories across the globe to observe this decay and the experiments are already in advanced stages of development. The most recent experimental results of  $0\nu\beta\beta$  decay of  $^{136}\text{Xe}$  have been reported by KamLand-Zen collaboration [1] and EXO 200 collaboration [2] and they give a lower limit of  $3.4 \times 10^{25}$  yr for the half-life. On the other hand, phase I results from GERDA experiment [3] for  $^{76}\text{Ge}$  are published recently giving a lower limit of  $3.0 \times 10^{25}$  yr for the half-life.

Nuclear transition matrix elements (NTME) are the essential ingredient for extracting the neutrino mass from the half lives. There has been considerable effort to obtain NTME for various candidate nuclei and they have been calculated theoretically using a variety of nuclear models: (i) large scale shell model (SM) [4]; (ii) quasi-particle random phase approximation (QRPA) and its variants [5–7]; (iii) proton-neutron interacting boson model (IBM-2) [8]; (iv) particle number and angular momentum projection including configuration mixing within the generating coordinate method framework (GCM+PNAMP) [9]; (v) projected Hartree-Fock-Bogoliubov (PHFB) method with pairing plus quadrupole quadrupole interaction [10]. Detailed comparative study of the results from these methods is discussed recently in [11, 12].

Besides the two electron mode, it is also possible to have neutrinoless positron double beta decay and this can come in three modes: (i) double  $\beta^+$  ( $\beta^+\beta^+$ ), (ii)  $\beta^+$  and electron capture ( $\beta^+\text{EC}$ ) and (iii) double electron capture (ECEC). The later process can proceed only by emission of extra particles or as a resonant process [13]. All these three modes combined are referred to as  $0\nu e^+DBD$ . There are now efforts to observe  $0\nu$  (and also  $2\nu$ )  $e^+DBD$  in some nuclei; see for example [14–16].

Over the last many years, the Deformed Shell Model (DSM) (based on Hartree-Fock

states) has been used to study various properties of nuclei in the mass  $A=60-90$  region (also in  $A=44-60$ ) with reasonable success. They include: (i) spectroscopic properties such as band structures, shapes and shape coexistence, nature of band crossings, electromagnetic transition probabilities [17–22]; (ii)  $T = 1$  and  $T = 0$  bands in  $N=Z$  odd-odd nuclei and  $T = 1/2$  bands in odd- $A$  nuclei by including isospin projection [23–25]; (iii) transition matrix elements for  $\mu - e$  conversion in  $^{72}\text{Ge}$  [26] and in the analysis of data for inelastic scattering of electrons from  $fp$ -shell nuclei [27]. More importantly, this model has also been used for studying  $2\nu$  double beta decay, in a first attempt, for  $^{76}\text{Ge} \rightarrow ^{76}\text{Se}$  in [28] with reasonable success. The DSM results for the spectroscopy of  $^{62}\text{Ga}$  have recently been compared with the predictions of spherical shell model [29]. The  $T = 0$  and  $T = 1$  energy levels and the isoscalar and isovector electromagnetic transition probabilities generated in both these models are found to be similar. Following this and the success of DSM in explaining spectroscopic properties of nuclei in  $A=60-90$  region, we have started a study of DBD in  $A=60-90$  nuclei.

As shown in table I, there are eight candidate nuclei in the  $A=60-90$  region with  $30 \leq Z \leq 40$  and  $N \leq 48$  which can undergo double beta decay. We have already applied DSM to study half lives for  $2\nu e^+\text{DBD}$  in  $^{78}\text{Kr}$  [30], in  $^{74}\text{Se}$  [31], in  $^{84}\text{Sr}$  [32] and in  $^{64}\text{Zn}$  [33]. Going further, more recently we have also calculated NTME for neutrinoless positron double beta decay  $0\nu\beta^+\beta^+$  and  $0\nu\beta^+\text{EC}$  for all the above four nuclei [33]. We ensured that DSM gives a good description of the spectroscopic properties for low-lying states for these nuclei. The deduced half-lives with these NTME, assuming neutrino mass is 1 eV, are smallest for  $^{78}\text{Kr}$  with half life for  $\beta^+\text{EC}$  decay being  $\sim 10^{27}$  yr. For all others, the half lives are in the range of  $\sim 10^{28}$  to  $10^{29}$  yr.

TABLE I: DBD candidates with  $A=60-90$ ,  $30 \leq Z \leq 40$  and  $N \leq 48$ .

$(0 + 2\nu)\beta^-\beta^-$	$(0 + 2\nu)e^+\text{DBD}$
$^{70}\text{Zn}$	$^{64}\text{Zn}$
$^{76}\text{Ge}$	$^{74}\text{Se}$
$^{80}\text{Se}$	$^{78}\text{Kr}$
$^{82}\text{Se}$	$^{84}\text{Sr}$

In addition to completing the study of the four candidate nuclei listed in Table I that undergo  $e^+\text{DBD}$ , in [33] we have also reported DSM results for  $0\nu$  DBD for  $^{76}\text{Ge}$ . With

this, we are left with the analysis of  $2\nu$  and  $0\nu$  DBD in  $^{70}\text{Zn}$ ,  $^{80}\text{Se}$  and  $^{82}\text{Se}$  nuclei (first DSM results for  $2\nu$  DBD for  $^{82}\text{Se}$  were given in [34]). Our purpose in the present paper is to present DSM results for these nuclei. We will give a preview.

In Section 2 discussed briefly are the formula for half life for  $0\nu\text{DBD}$ , the transition operator generating NTME and the DSM model. Section 3 gives DSM results for  $^{70}\text{Zn}$  first for spectroscopic properties and then the results for both  $2\nu$  and  $0\nu$  double beta decay half lives. In Section 4, DSM results for  $2\nu$  and  $0\nu$  double beta decay half lives for  $^{80}\text{Se}$  are given and similarly in Section 5 for  $^{82}\text{Se}$ . Not many theoretical calculations of spectroscopic properties of  $^{70}\text{Zn}$  are available in the literature. Our results obtained using DSM are presented in Section 3. Also, DSM results for orbit occupancies for all the three nuclei are discussed in Sections 3-5. Finally, Section 6 gives conclusions.

## II. FORMALISM

### A. $0\nu\text{DBD}$ half life and transition operator

Half-life for  $0\nu\text{DBD}$  for the  $0_i^+$  ground state (gs) of a initial even-even nucleus decaying to the  $0_f^+$  gs of the final even-even nucleus is given by [11]

$$[T_{1/2}^{k:0\nu}(0_i^+ \rightarrow 0_f^+)]^{-1} = G^{0\nu}(k) (g_A)^4 |M^{0\nu}(0^+)|^2 \left( \frac{\langle m_\nu \rangle}{m_e} \right)^2, \quad (1)$$

where  $\langle m_\nu \rangle$  is the effective neutrino mass (a combination of neutrino mass eigenvalues and it also involves neutrino mixing matrix) and  $k$  denotes the decay mechanism (light neutrino exchange, heavy neutrino exchange and Majoron emission - in the present paper light neutrino exchange is assumed). The  $G^{0\nu}(k)$  is phase space integral (kinematical factor) dependent on charge, mass and available energy for the  $0\nu\text{DBD}$  process. In Eq. (1), the  $M^{0\nu}$  is the nuclear transition matrix element (NTME) of the  $0\nu\text{DBD}$  transition operator and it is a sum of a Gamow-Teller like ( $M_{GT}$ ), Fermi like ( $M_F$ ) and tensor ( $M_T$ ) two-body operators. As it is well known that the tensor part contributes only up to 10% of the matrix elements [11], we will neglect the tensor part. Then we have, from the closure approximation which

is well justified for  $0\nu\text{DBD}$ ,

$$\begin{aligned} M^{0\nu}(0^+) &= M_{GT}^{0\nu}(0^+) - \frac{g_V^2}{g_A^2} M_F^{0\nu}(0^+) = \langle 0_f^+ \parallel \mathcal{O}(2 : 0\nu) \parallel 0_i^+ \rangle, \\ \mathcal{O}(2 : 0\nu) &= \sum_{a,b} \mathcal{H}(r_{ab}, \overline{E}) \tau_a^+ \tau_b^+ \left( \sigma_a \cdot \sigma_b - \frac{g_V^2}{g_A^2} \right). \end{aligned} \quad (2)$$

Note that  $\tau^+$  changes a neutron into a proton. As seen from Eq. (2),  $0\nu\text{DBD}$  half-lives are generated by the two-body transition operator  $\mathcal{O}(2 : 0\nu)$ ; note that  $a, b$  label nucleons. The  $g_A$  and  $g_V$  are the weak axial-vector and vector coupling constants. The  $\mathcal{H}(r_{ab}, \overline{E})$  in Eq. (2) is the ‘neutrino potential’. Here  $\overline{E}$  is the average energy of the virtual intermediate states used in the closure approximation [11, 35–38]. The form given by Eq. (2) is justified *only if the exchange of the light Majorana neutrino is indeed the mechanism responsible for the  $0\nu\text{DBD}$* . The effects of short-range correlations in the wave functions are taken into account by multiplying the wave function by the Jastrow function  $[1 - \gamma_3 e^{-\gamma_1 r_{ab}^2} (1 - \gamma_2 r_{ab}^2)]$  [36, 38]. Now keeping the wave functions unaltered, the Jastrow function can be incorporated into  $\mathcal{H}(r_{ab}, \overline{E})$  giving an effective  $\mathcal{H}_{eff}(r_{ab}, \overline{E})$ ,

$$\mathcal{H}(r_{ab}, \overline{E}) \rightarrow \mathcal{H}_{eff}(r_{ab}, \overline{E}) = C_0 \times \mathcal{H}(r_{ab}, \overline{E}) [1 - \gamma_3 e^{-\gamma_1 r_{ab}^2} (1 - \gamma_2 r_{ab}^2)]^2. \quad (3)$$

The values chosen for the parameters  $\gamma_1$ ,  $\gamma_2$  and  $\gamma_3$  are given below. The value of the constant  $C_0$  is found to be 3 by comparing the calculated half-lives and the shell model value for half lives for  $^{76}\text{Ge}$  as has been discussed in detail in [33]. This constant is used to renormalize the  $0\nu$  nuclear matrix elements. As seen ahead, the model reproduces reasonably well the spectroscopy of the parent and daughter nuclei. It also describes  $2\nu$  half lives. But the model under estimates the spherical shell model calculated nuclear matrix elements by a factor of 3. The reasons can be two fold. One possibility is the limited number of configurations taken in our calculation unlike shell model. Another plausible reason is that shell model uses different effective interaction and these effective interactions are not available in the literature. As shown in [11], the nuclear matrix elements in different models already differ by as much as by a factor of 3. Hence essential physics will not be lost if we renormalize the nuclear matrix elements by a scale factor of 3.

There are a number of parameters in the  $0\nu\text{DBD}$  transition operator and the choices made for the various parameters are: (i)  $R = 1.2A^{1/3}$  fm; (ii)  $b = 1.003A^{1/6}$  fm [11]; (iii)  $\overline{E} = 1.12A^{1/2}$  MeV [37]; (iv)  $g_A/g_V = 1.254$ ; (v)  $(\gamma_1, \gamma_2, \gamma_3)$  in Eq. (3) are (1.1, 0.68, 1) [Miller-Spencer] [38, 39].

There are other methods, besides using Jastrow function as in Eq. (3), to take into account the short range correlations. The unitary correlation operator method (UCOM) [40] recently developed by Kortelainen et al. is one such effort. It has been shown that the Jastrow method exaggerates the effects of short-range correlations. For example in  $^{48}\text{Ca}$  and  $^{76}\text{Ge}$ , the Jastrow method has been found to lead to reduction of 30%-40% in the magnitude of nuclear matrix elements whereas in UCOM, the reduction is 7%-16%. The calculation using this method will be carried out in a separate publication.

Now we will discuss briefly the deformed shell model formulation for calculating NTME.

## B. DSM model

In DSM, for a given nucleus, starting with a model space consisting of a given set of single particle (sp) orbitals and effective two-body Hamiltonian, the lowest energy intrinsic states are obtained by solving the Hartree-Fock (HF) single particle equation self-consistently. Excited intrinsic configurations are obtained by making particle-hole excitations over the lowest intrinsic state. These intrinsic states  $\chi_K(\eta)$  do not have definite angular momenta. and states of good angular momentum projected from an intrinsic state  $\chi_K(\eta)$  can be written in the form

$$\psi_{MK}^J(\eta) = \frac{2J+1}{8\pi^2\sqrt{N_{JK}}} \int d\Omega D_{MK}^{J*}(\Omega) R(\Omega) |\chi_K(\eta)\rangle \quad (4)$$

where  $N_{JK}$  is the normalization constant given by

$$N_{JK} = \frac{2J+1}{2} \int_0^\pi d\beta \sin \beta d_{KK}^J(\beta) \langle \chi_K(\eta) | e^{-i\beta J_y} | \chi_K(\eta) \rangle. \quad (5)$$

In Eq. (4)  $\Omega$  represents the Euler angles  $(\alpha, \beta, \gamma)$ ,  $R(\Omega)$  which is equal to  $\exp(-i\alpha J_z)\exp(-i\beta J_y)\exp(-i\gamma J_z)$  represents the general rotation operator. The good angular momentum states projected from different intrinsic states are not in general orthogonal to each other. Hence they are orthonormalized and then band mixing calculations are performed. For details see [33].

DSM is well established to be a successful model for transitional nuclei (with  $A=60-90$ ) when sufficiently large number of intrinsic states are included in the band mixing calculations. Performing DSM calculations for the parent and daughter and then using the DSM wave functions, the  $\mathcal{O}(2 : 0\nu)$  operator matrix elements are calculated and the results are presented in the next three Sections.

### III. $^{70}\text{Zn}$ RESULTS

#### A. Spectroscopic properties

The double beta decay of  $^{70}\text{Zn}$  has recently been studied experimentally by Belli et al [14] (they set the lower limits to the half life for neutrinoless DBD to be  $3.2 \times 10^{19}$  yr at 90% C.L.). Its natural isotopic abundance is 0.62%. Before going to double beta decay, we will first study its spectroscopic properties using DSM model to test the goodness of the model for this nucleus.

$^{70}\text{Zn}$  with 30 protons and 40 neutrons lie near the proton shell closure and neutron sub-shell closure. The daughter nucleus  $^{70}\text{Ge}$  has two neutrons less and two protons more. The spectra of ground state bands for both the nuclei are similar. The energy levels are more or less equispaced. As discussed in Sect. II.B., we first carry out an axially symmetric HF calculation for each nucleus using the newly developed jj44b effective interaction [41] within the model space consisting of the orbitals  $^2p_{3/2}$ ,  $^1f_{5/2}$ ,  $^2p_{1/2}$  and  $^1g_{9/2}$  with  $^{56}\text{Ni}$  as the core. It should be mentioned that the same model space was used in many recent shell model and interacting boson model calculations [11, 42–46] for  $^{76}\text{Ge}$  and  $^{82}\text{Se}$  nuclei and  $^{70}\text{Zn}$  is in the same region. The spherical single particle energies for these orbits are taken as -9.6566, -9.2859, -8.2695 and -5.8944 MeV and are kept same both for protons as well as neutrons. In the past we have performed many calculations in this region using a modified Kuo interaction. However,  $^{70}\text{Zn}$  lies very close to the proton shell closure and the modified Kuo interaction has been found to be inadequate for this nucleus. Hence we study this nucleus using the jj44b effective interaction developed by Brown and his group [41]. The lowest energy HF solutions for  $^{70}\text{Zn}$  and its daughter nucleus  $^{70}\text{Ge}$  are shown in Fig. 1. The two active protons in  $^{70}\text{Zn}$  occupy the lowest  $k = 1/2^-$  orbital. There is a well defined gap of 3.7 MeV above the proton Fermi surface. The neutron gap above the neutron Fermi surface is 1.3 MeV. As a result,  $^{70}\text{Zn}$  has relatively stable deformation in the ground state. As discussed before, particle-hole excitations over the lowest HF solution are carried out and generated a total of 226 intrinsic states (with  $K = 0^+$  and  $K \neq 0^+$  up to 6 MeV excitation). Angular momentum projection from each of these intrinsic states is carried out and then a band mixing calculation is performed. The calculated levels are classified on the basis of their  $B(E2)$  values and also the structure of the levels.

The single particle spectrum for the lowest energy HF solution for the daughter nucleus  $^{70}\text{Ge}$  is also shown in figure 1. The proton and neutron gaps above their respective Fermi surfaces are less than 1 MeV. Hence one can easily excite protons and neutrons above their Fermi surfaces. We have considered 180 configurations with  $K = 0^+$  and  $K \neq 0^+$  up to 6 MeV excitation. Good angular momentum states are projected from each of these intrinsic states and then a band mixing calculation is performed to orthonormalize these projected states. The calculated levels having similar structure and connected by relatively large  $B(E2)$  are classified as belonging to one band.

The calculated levels and the bands for  $^{70}\text{Zn}$  and  $^{70}\text{Ge}$  are compared with experiment in Figs. 2 and 3. The experimental data for the two nuclei are taken from [47]. The calculated spectrum is compressed compared to experiment. Except for the  $2^+ \rightarrow 0^+$  separation, the relative spacing of all the other levels are reasonable. The ground band in both nuclei is mainly an admixture of the lowest intrinsic configuration at low spin. However at higher spins, there is mixing due to other configurations. The quasi-gamma bands in both the nuclei are also compared with experiment. The quantities near the arrows represent  $B(E2)$  values in W.u. unit. The agreement with experiment for the  $B(E2)$  values is quite satisfactory. The  $B(E2)$  values are calculated with effective charges of  $e_p=1.5$  and  $e_n=0.5$ . The  $B(E2)$  values provide a test of the goodness of nuclear wave functions generated in the model. In view of the good agreement, we have confidence about the suitability of the model for studying double beta decay properties.

Going beyond these, orbit occupancies for protons and neutron for these nuclei are presented in Fig. 4. It is important to add that, recently there has been experimental efforts to measure the population of the valence orbits in several double beta decay candidate nuclei [48–52]. It will be quite useful if single nucleon transfer experiments are performed for  $^{70}\text{Zn}$  and  $^{70}\text{Ge}$  nuclei to test these results.

## B. $2\nu$ DBD half lives and $0\nu$ DBD NTME and half lives

First we will consider  $2\nu$  DBD and the half-life for the  $0_I^+ \rightarrow 0_F^+$  double beta decay is given by [53]

$$[T_{1/2}^{2\nu}]^{-1} = G_{2\nu} |M_{2\nu}|^2 \quad (6)$$



The kinematical factor  $G_{2\nu}$  is independent of nuclear structure and its value  $G_{2\nu} = 0.32 \times 10^{-21} \text{ yr}^{-1}$  [53]). On the other hand, the nuclear transition matrix elements (NTME)  $M_{2\nu}$  are nuclear model dependent and they are given by,

$$M_{2\nu} = \sum_N \frac{\langle 0_F^+ || \sigma \tau^+ || 1_N^+ \rangle \langle 1_N^+ || \sigma \tau^+ || 0_I^+ \rangle}{[E_N - (E_I + E_F)/2] / m_e} \quad (7)$$

where  $|0_I^+\rangle$ ,  $|0_F^+\rangle$  and  $|1_N^+\rangle$  are the initial, final and virtual intermediate states respectively and  $E_N$  are the energies of the intermediate nucleus  $^{70}\text{Ga}$ . Similarly  $E_I$  and  $E_F$  are the ground state energies of the parent and daughter nuclei. We have from [54], the atomic masses of  $^{70}\text{Zn}$ ,  $^{70}\text{Ga}$  and  $^{70}\text{Ge}$  to be  $-69.5646$ ,  $-68.9101$  and  $-70.5631$  MeV respectively (for nuclear mass, we need to subtract the mass of the electrons from the atomic mass). For  $^{70}\text{Ga}$ ,  $1^+$  is the ground state. Then, with  $E_{1+}$  denoting the relative energies of the  $1^+$  states in  $^{70}\text{Ga}$  with respect to the lowest  $1^+$  state, we finally obtain  $[E_N - (E_I + E_F)/2] = [1.1537 + E_{1+}]$  MeV. DSM is used to calculate  $E_{1+}$ . The nuclear matrix elements given ahead correspond to the values of  $M_{2\nu}$  with  $m_e=1$ .

In the DSM calculations we have considered 30 lowest intrinsic states with  $K = 0^+$  for  $^{70}\text{Zn}$ , 26 lowest intrinsic configurations with  $K = 0^+$  for the daughter nucleus  $^{70}\text{Ge}$  and 65 intrinsic states with  $K = 1^+$  or  $K = 0^+$  for the intermediate nucleus  $^{70}\text{Ga}$ . The intrinsic states with  $K = 1^+$  or  $K = 0^+$  for  $^{70}\text{Ga}$  are generated by making particle-hole excitations over the lowest HF intrinsic state generated for this nucleus. We project out  $1^+$  states from each of these intrinsic states and then perform a band mixing calculation as discussed above. Taking the phase space factor  $0.32 \times 10^{-21} \text{ yr}^{-1}$  [53] the DSM value for the  $2\nu$  DBD half-life is  $3.39 \times 10^{23}$ . Bobyk et al [55] have evaluated the half life for the  $2\nu\beta\beta$  decay using different variants of QRPA with different values of  $g_{ph}$  and  $g_{pp}$  and their value varies from  $5 \times 10^{20}$  to  $6.4 \times 10^{23}$ . Our calculated half life lies near the value in the upper limit. In our calculation, the nuclear matrix element  $M_{2\nu}$  comes out to be  $0.19 \text{ MeV}^{-1}$  which is smaller than the value given by Suhonen [56] by a factor of around 2.4. The contributions to the nuclear matrix element by the first two  $1^+$  states of the intermediate nucleus are  $0.058$  and  $0.095 \text{ MeV}^{-1}$ , respectively. Thus these two states contribute predominately to the nuclear matrix element and this is close to the single-state dominance predicted in [57].

Spectroscopic results and  $2\nu\text{DBD}$  half lives show that we can use DSM for reliable predictions for  $0\nu$  DBD. Turning to this, in the calculation of half-lives for  $0\nu$  DBD we have considered 30 intrinsic states with  $K = 0^+$  for  $^{70}\text{Zn}$  and 26 intrinsic configurations with

$K = 0^+$  for the daughter nucleus  $^{70}\text{Ge}$  as in  $2\nu$  case. The calculated NTME for  $^{70}\text{Zn}$  is 1.99. The GT contribution is 1.748 and the Fermi part is -0.379. We see that the Fermi matrix element is small compared to the GT matrix element and hence there is no isospin contamination although we have used proton-neutron formulation in DSM without isospin projection. In Table II, the DSM value for  $M^{0\nu}$  is compared with the available QRPA values [56] obtained with different  $g_A$  values and different sets of single particle energies for the orbits chosen in the calculations. The values with  $g_A = 1.25$  are close to the DSM values. Now, using Eq. (1), taking the neutrino mass to be 1 eV and the phase space factor  $0.23 \times 10^{-26} \text{ yr}^{-1}$  from [53], the calculated half-life from DSM for  $0\nu\beta\beta$  decay is  $1.1 \times 10^{26} \text{ yr}$  (note that in [53], the factors  $(g_A)^4$  and  $(m_e)^2$  appearing in Eq. (1) are absorbed in the phase space factor  $G^{0\nu}$ ). At present very low lower bounds ( $\geq 3.2 \times 10^{19} \text{ yr}$  at 90% C.L.) for the  $0\nu$  DBD half life for  $^{70}\text{Zn}$  is known from experiments [14]. The half-lives are displayed in table II.

#### IV. $^{80}\text{Se}$ RESULTS

##### A. Spectroscopic properties

In the double beta decay of  $^{80}\text{Se}$ , the daughter nucleus is  $^{80}\text{Kr}$ . As in the case of  $^{70}\text{Zn}$ , we will first consider spectroscopic properties of these nuclei before discussing the double beta decay results. Both the nuclei are studied using the modified Kuo effective interaction given in [58] in the model space consisting of the single particle orbitals  $^2p_{3/2}$ ,  $^1f_{5/2}$ ,  $^2p_{1/2}$  and  $^1g_{9/2}$  with  $^{56}\text{Ni}$  as the core. This effective interaction was used by us in most of our calculations for  $A=60-90$  nuclei. The spherical single particle energies for these orbitals are taken as 0.0, 0.78, 1.08 and 4.25 MeV for protons and 0.0, 0.78, 1.58 and 2.75 MeV for neutrons. It may be mentioned that we had performed a preliminary study of the spectroscopy of  $^{80}\text{Kr}$  and  $^{82}\text{Kr}$  [59] with spherical single particle energies of neutrons to be same as protons taken above. However the present set of single particle energies gives much better description of spectroscopic properties. The HF single particle spectrum for these two nuclei are given in Fig. 5. For  $^{80}\text{Se}$ , there is a well defined gap of 2.3 MeV above the proton Fermi surface and the gap above the neutron Fermi surface is 1.2 MeV. Thus,  $^{80}\text{Se}$  has a relatively stable shape. On the other hand, for  $^{80}\text{Kr}$ , the proton and neutron gaps above their respective

Fermi surfaces are much smaller. For studying spectroscopic properties of  $^{80}\text{Se}$ , we have considered 10 intrinsic states (including the lowest one). The excited configurations are obtained by making particle-hole excitations over the lowest configuration. As discussed above, good angular momentum states are projected from each of these intrinsic states and then these good  $J$  states are orthonormalized. The calculated spectrum is compared with experiment in Fig. 6. The agreement is quite satisfactory for the ground band. The  $B(E2)$  values are given near the arrows in the figure and the known  $B(E2)$ s are well reproduced. In order to study the energy spectrum of the daughter nucleus  $^{80}\text{Kr}$ , we have considered a total of 12 intrinsic states, the excited ones are obtained by particle-hole excitation. The energy spectrum obtained after angular momentum projection and band mixing is shown in Fig. 7. Experimentally for this nucleus, the ground band up to  $J = 10^+$  and a quasi-gamma band have been observed. This nucleus shows three  $8^+$  and two  $10^+$  levels. The ground band and the quasi-gamma band are quite well reproduced in our calculation. We find that a proton aligned band crosses the ground band at  $J = 10^+$ . In addition, we predict an excited  $K = 0^+$  band. In our calculation, we also obtain three close lying  $8^+$  and two close lying  $10^+$  levels as in the experiment. We have calculated  $B(E2)$  values for all possible transitions. The comparison with experiment for some of the  $B(E2)$  values are given in Table III. In the calculation of  $B(E2)$ , we have used the effective charges 1.6 and 1.0 for protons and neutrons as in our earlier calculations with this effective interaction. For both the nuclei, we have also calculated the orbit occupancies and they are displayed in Fig. 4.

### B. $2\nu$ DBD half lives and $0\nu$ DBD NTME and half lives

The  $2\nu\beta\beta$  decay for this nucleus is studied using the Eqns. 6 and 7. The atomic masses of  $^{80}\text{Se}$ ,  $^{80}\text{Kr}$  and the intermediate nucleus  $^{80}\text{Br}$  are -77.7599, -77.8925 and -75.8895 MeV respectively as given in [54]. For the intermediate nucleus  $^{80}\text{Br}$ ,  $1^+$  is the ground state. Taking  $E_{1^+}$  to be the calculated energies of  $^{80}\text{Br}$  with respect to the lowest  $1^+$ , the energy denominator is given by  $[E_N - (E_I + E_F)/2] = [1.9367 + E_{1^+}]$  MeV. DSM is used to calculate  $E_{1^+}$ . In the DSM calculation for  $2\nu\beta\beta$ , we have considered 13 configurations for  $^{80}\text{Se}$ , 55 configurations for the daughter nucleus  $^{80}\text{Kr}$ , all with  $K = 0^+$ . For the intermediate nucleus  $^{80}\text{Br}$ , we considered 99 configurations with  $K = 1^+$  or  $K = 0^+$ . For the odd-odd nucleus like  $^{80}\text{Br}$ , the configurations with  $K = 0^+$  can also give  $1^+$  levels. We project out  $0^+$  levels

for the parent and daughter nuclei and then orthonormalize them separately. Similarly, for the intermediate nucleus  $^{80}\text{Br}$ , we project out  $1^+$  levels from all the configurations and then orthonormalize them. The calculated half life with phase space factor  $0.12 \times 10^{-27}$  [53] comes out to be  $1.97 \times 10^{29}$  yr. This value agrees quite well with the QRPA result quoted by Bobyk et al. [55]. The nuclear matrix element  $M_{2\nu}$  is  $0.40 \text{ MeV}^{-1}$ . The contribution to the nuclear matrix element from the first two  $1^+$  states of the intermediate nucleus is 0.038 and 0.288  $\text{MeV}^{-1}$ . The contribution of other  $1^+$  states are more than 10 times smaller. Thus, this nucleus shows the single-state dominance in the  $2\nu\beta\beta$  decay transition as predicted in [57].

Then we proceed to calculate the nuclear matrix element for neutrinoless double beta decay. As above we considered 13 configurations for the parent nucleus  $^{80}\text{Se}$  and 55 intrinsic states for the daughter nucleus  $^{80}\text{Kr}$ . The  $0\nu\beta\beta$  nuclear matrix element comes out to be 3.19. The GT and the Fermi matrix elements contributing to the above NTME are found to be 2.684 and -0.801, respectively. Here also we find that the Fermi matrix element is substantially smaller than the GT matrix element indicating that there is no isospin contamination. Also, to our knowledge there are no other model calculations available for  $M^{0\nu}$  for  $^{80}\text{Se}$ . Going further, taking the neutrino mass to be 1 eV and phase space factor  $0.43 \times 10^{-28} \text{ yr}^{-1}$  [53], the half-life is  $2.3 \times 10^{27}$  yr. The half-lives are displayed in table II.

## V. $^{82}\text{SE}$ RESULTS

### A. Spectroscopic properties

As in the case of  $^{80}\text{Se}$ , we perform the calculation of  $^{82}\text{Se}$  and the daughter nucleus  $^{82}\text{Kr}$  using the modified Kuo effective interaction in the model space consisting of the single particle orbitals  $^2p_{3/2}$ ,  $^1f_{5/2}$ ,  $^2p_{1/2}$  and  $^1g_{9/2}$  with  $^{56}\text{Ni}$  as the core. The spherical single particle energies for these orbitals are taken as 0.0, 0.78, 1.08 and 4.25 MeV for protons and 0.0, 0.78, 1.58 and 2.75 MeV for neutrons. As mentioned earlier, the same model space was used in many shell model and IBM calculations [11, 42–46]. As before, we first perform axially symmetric HF calculation for both the nuclei and obtain the lowest energy prolate solution. The lowest energy prolate solution is shown in Fig. 8.  $^{82}\text{Se}$  also has a well defined gap 2.1 MeV and 3.2 MeV above the proton and neutron Fermi surfaces and hence it has a stable shape. However for the daughter nucleus  $^{82}\text{Kr}$ , the gaps are much smaller. The proton gap

is only 0.9 MeV whereas the neutron gap is 1.8 MeV. For calculating the energy spectrum, we perform particle-hole excitations over the lowest HF configuration for each nucleus and obtain excited intrinsic states. Good angular momentum states are projected from each of these intrinsic states. These good angular momentum states are then orthonormalized and then a band mixing calculation is performed. For studying the energy spectrum of  $^{82}\text{Se}$ , we considered 10 intrinsic states. The energy spectrum is given in Fig. 9. The ground band is quite well reproduced in our calculation. We find that a neutron aligned band crosses the ground band at  $J = 8^+$ . Recently we had studied the  $2\nu\beta\beta$  decay of this nucleus [34] using a slightly different set of spherical single particle energies. The energy spectrum is more or less similar to the present case. We have calculated  $B(E2)$  values for all possible transitions taking effective charges 1.6 and 1.0 for protons and neutrons. In the ground band, only two  $B(E2)$  transitions are known and they are in good agreement with DSM values as shown in Fig. 9.

For calculating the spectroscopic properties of the daughter nucleus  $^{82}\text{Kr}$ , we have considered 12 intrinsic states. After angular momentum projection and orthonormalization, the energy bands obtained in our calculation are compared in Fig. 10. The ground band and the quasi-gamma band are quite nicely reproduced in our calculation. We calculate the  $B(E2)$  values with the same effective charges as in  $^{80}\text{Se}$ . The  $B(E2)$  values are compared with experiment in table III. The agreement is quite satisfactory.

### B. $2\nu$ DBD half lives and $0\nu$ DBD NTME and half lives

The  $2\nu$  DBD for  $^{82}\text{Se}$  is first studied using Eqns. 6 and 7. We have considered 7 intrinsic states for  $^{82}\text{Se}$  and 48 intrinsic states for the daughter nucleus  $^{80}\text{Kr}$  all with  $K = 0^+$ .  $J = 0^+$  states are projected out from each of these intrinsic states and then these states are orthonormalized for each nucleus. The intermediate nucleus  $^{82}\text{Br}$  generates the  $1^+$  states. Excited configurations with  $K = 0^+$  and  $K = 1^+$  for the intermediate nucleus are obtained by making particle-hole excitations over the lowest HF intrinsic configuration. Then we perform angular momentum projection to project out  $J = 1^+$  levels from each intrinsic state. These angular momentum states are then orthonormalized. We took 83 configurations with  $K = 0^+$  or  $K = 1^+$  and calculated the numerator of Eq. (7). The atomic masses for the parent, intermediate and daughter nuclei are -77.5940, -77.4965 and -80.5895 MeV

respectively [54]. For this nucleus, the lowest  $1^+$  state is at an excitation of 0.075 MeV. If  $E_{1+}$  are the energies of the excited  $1^+$  states with respect to the lowest one which are calculated within our DSM model, the energy denominator is given by  $(1.6702 + E_{1+})$ . With the phase space factor  $0.43 \times 10^{-17} \text{ yr}^{-1}$  [53], we predict the half life to be  $1.58 \times 10^{19} \text{ yr}$  compared to the experimental value  $(0.92 \pm 0.07) \times 10^{20} \text{ yr}$ . Thus our calculated value is about 6 times smaller than experiment. Similar effect was seen by Caurier et al [60] in their shell model calculation and hence they have to introduce a quenching factor of 0.60. If we use this factor, our half life is close to the shell model value. The nuclear matrix element is  $0.24 \text{ MeV}^{-1}$ . The contribution of the first  $1^+$  state of the intermediate nucleus to the nuclear matrix element is  $0.21 \text{ MeV}^{-1}$  which is predominant. The contribution of the other  $1^+$  states to the nuclear matrix element is more than 10 times smaller. Thus this nucleus also exhibits single-state dominance in  $2\nu\beta\beta$  decay transitions as predicted in ref. [57].

Then we proceed to calculate the neutrinoless double beta decay half life. We take 7 configurations for the parent nucleus  $^{82}\text{Se}$  and 48 configurations for the daughter nucleus  $^{82}\text{Kr}$  as in the two neutrino case with  $K = 0^+$ . Good  $J = 0^+$  states are projected from these intrinsic states and they are orthonormalized by performing band mixing calculation for each nucleus. The calculated nuclear matrix element is 2.04. The GT contribution is found to be 1.853 and the Fermi matrix element whose magnitude is smaller than the GT matrix element is -0.296. Taking the phase space factor  $0.11 \times 10^{-24} \text{ yr}^{-1}$  [53] and the neutrino mass to be 1eV, the half life is  $2.2 \times 10^{24} \text{ yr}$ . The half lives are presented in table II. It should be added that there is considerable interest in  $^{82}\text{Se}$  because of the upcoming SuperNEMO experiment [61]. The NEMO-3 gave a lower limit of  $3.2 \times 10^{23} \text{ yr}$  at 90% C.L. for this nucleus [61].

With SuperNEMO coming soon, new large scale shell model calculations are being carried out [43]. There are also predictions for  $M^{0\nu}$  from many other nuclear models as shown in Table II and the results are as follows. Shell model values range from 2.18 to 3.39 [4, 43, 64] and the current expectation is that its value should be  $3.3 \pm 0.1$  as quoted in [43]. The DSM value as given above is 2.04 and it is smaller than the SM value. Similarly, various QRPA calculations give  $M^{0\nu}$  in the range 2.77 to 5.65 [7, 12, 38, 65]. The current value from QRPA with Jastrow short range correlations is  $M^{0\nu} = 3.15 \pm 0.3$  and from UCOM correlations is  $4.2 \pm 0.35$  [12]. Finally the values from IBM-2 model are 4.41 to 4.84 [8, 11, 46] and from GCM+PNAMP model is 4.22 [9].

## VI. CONCLUSIONS

In the  $A=60-90$  region with  $30 \leq Z \leq 40$  and  $N \leq 48$  there are eight candidate nuclei, as shown in Table I, which can undergo double beta decay. Prompted by the success of deformed shell model, based on Hartree-Fock intrinsic states with band mixing, in explaining spectroscopic properties of nuclei in the  $A=60-90$  region, recently DSM results for the four  $0\nu e^+DBD$  candidate nuclei, i.e.  $^{64}\text{Zn}$ ,  $^{74}\text{Se}$ ,  $^{78}\text{Kr}$  and  $^{84}\text{Sr}$  have been reported by us in [33]. Similarly the results for  $2\nu e^+DBD$  half lives are reported in [30–33]. In addition, results for  $2\nu$  and  $0\nu DBD$  for  $^{76}\text{Ge}$  have been reported in [28] and [33] respectively. Complementing this work, in the present paper DSM results for  $0\nu DBD$  for the three remaining nuclei, i.e. for  $^{70}\text{Zn}$ ,  $^{80}\text{Se}$  and  $^{82}\text{Se}$  are presented. After ensuring reasonable DSM description of spectroscopic properties that include spectra and  $B(E2)$ 's, we have presented the results for occupancies for the parent and daughter nuclei involved. Proceeding further, DSM results for NTME and there by for the  $0\nu DBD$  half-lives are presented for  $^{70}\text{Zn}$ ,  $^{80}\text{Se}$  and  $^{82}\text{Se}$  as shown in Table II. The present paper brings to conclusion DSM study of the eight DBD candidate nuclei listed in Table I. Future DSM studies call for using much larger set of single particle levels, suitable effective interactions in the larger spaces and inclusion of much larger number of intrinsic states in band mixing calculations. The present model space has also been used in many shell model [42–45] and interacting boson model studies [11, 46]. We plan to expand the model space in future to include much larger number of spin-orbit partners so that the Ikeda sum rule is well satisfied and also carry out an analysis of (p,n) GT strength functions and beta decay data involving  $0\nu$  and  $2\nu DBD$  nuclei.

Before concluding, we mention that recently we have also studied the role of deformation in generating NTME for  $0\nu DBD$  within DSM framework. Towards this end we have considered  $^{70}\text{Zn}$  and  $^{150}\text{Nd}$  nuclei as examples and employed for each of these two different effective interactions that produce spherical and well deformed shape respectively. These calculations clearly showed that deformation reduces NTME by a factor of 2-3; see [66] for details. In a different approach, Menéndez et al [64] examined pairing effects (where the shape is close to spherical) versus deformation within shell model by analyzing the evolution of NTME with the maximum seniority permitted in the wavefunctions.

## Acknowledgments

RS is thankful to DST (Government of India) for financial support. RS and VKBK thank H.J. Kim, KNU, South Korea for his interest in the present work. Thanks are also to the referee for many useful comments.

- 
- [1] A. Gando *et al.*, Phys. Rev. Lett. **110**, 062502 (2013).
  - [2] M. Auger *et al.*, Phys. Rev. Lett. **109**, 032505 (2012).
  - [3] M. Agostini *et al.*, Phys. Rev. Lett. **111**, 122503 (2013).
  - [4] E. Caurier, J. Menéndez, F. Nowacki, and A. Poves, Phys. Rev. Lett. **100**, 052503 (2008)
  - [5] F. Šimkovic, A. Faessler, V. Rodin, P. Vogel and J. Engel, Phys. Rev. C **77**, 045503 (2008)
  - [6] D.-L. Fang, A. Faessler, V. Rodin and F.Šimkovic, Phys. Rev. C **83**, 034320 (2011)
  - [7] M. Kortelainen and J. Suhonen, Phys. Rev. C **75**, 051303(R) (2007).
  - [8] J. Barea, J. Kotila, and F. Iachello, Phys. Rev. Lett. **109**, 042501 (2012).
  - [9] T.R. Rodríguez and G. Martinez-Pinedo, Phys. Rev. Lett. **105**, 252503 (2010)
  - [10] K. Chaturvedi, R. Chandra, P.K. Rath, P.K. Raina, and J.G. Hirsch, Phys. Rev. C **78**, 054302 (2008)
  - [11] J. Barea, J. Kotila, and F. Iachello, Phys. Rev. C **87**, 014315 (2013).
  - [12] J. Suhonen and O. Civitarese, J. Phys. G **39**, 124005 (2012).
  - [13] J. Suhonen, Eur. Phys. J. A **48**, 51 (2012)
  - [14] B P. Belli *et al.*, J. Phys. G: Nucl. Part. Phys. **38**, 115107 (2011).
  - [15] A.S. Barabash, P. Hubert, A. Nachab, and V. Umatov, Nucl. Phys. A **785**, 371 (2007).
  - [16] [http://www.apctp.org/topical/2009/npap2009/Presentations/APCTP\\_NPAP2009\\_192\\_Kim.pdf](http://www.apctp.org/topical/2009/npap2009/Presentations/APCTP_NPAP2009_192_Kim.pdf)
  - [17] R. Sahu and S.P. Pandya, J. Phys. G **14**, L165 (1988).
  - [18] R. Sahu and S.P. Pandya, Nucl. Phys. **A548**, 64 (1992).
  - [19] K.C. Tripathy and R. Sahu, J. Phys. G **20**, 911 (1994).
  - [20] R. Sahu and S.P. Pandya, Nucl. Phys. **A571**, 253 (1994).
  - [21] K. C. Tripathy and R. Sahu, Nucl. Phys. **A597**, 177 (1996).
  - [22] K.C. Tripathy and R. Sahu, Int. J. Mod. Phys. E **11**, 531 (2002).



- [23] R. Sahu and V.K.B. Kota, Phys. Rev. **C 66**, 024301 (2002).
- [24] R. Sahu and V.K.B. Kota, Phys. Rev. **C 67**, 054323 (2003).
- [25] S. Mishra, R. Sahu, and V.K.B. Kota, Prog. Theo. Phys. **118**, 59 (2007).
- [26] T.S. Kosmas, A. Faessler, and R. Sahu, Phys. Rev. C **68**, 054315 (2003).
- [27] R. Sahu, K.H. Bhatt, and D.P. Ahalpara, J. Phys. G **16**, 733 (1990).
- [28] R. Sahu, F. Šimkovic, and A. Faessler, J. Phys. G **25**, 1159 (1999).
- [29] P.C. Srivastava, R. Sahu and V.K.B. Kota, Eur. Phys. J. A **51**: 3 (2015).
- [30] S. Mishra, A. Shukla, R. Sahu, and V.K.B. Kota, Phys. Rev. C **78**, 024307 (2008).
- [31] A. Shukla, R. Sahu and V.K.B. Kota, Phys. Rev. C **80**, 057305 (2009).
- [32] R. Sahu and V.K.B. Kota, Int. J. Mod. Phys. E **20**, 1723 (2011).
- [33] R. Sahu, P.C. Srivastava and V.K.B. Kota, J. Phys. G **40**, 095107 (2013)
- [34] R. Sahu, P.C. Srivastava and V.K.B. Kota, Can. J. Phys. **89**, 1101 (2011)
- [35] J. Kotila and F. Iachello, Phys. Rev. C **87**, 024313 (2013).
- [36] J. Engel, P. Vogel and M. R. Zirnbauer, Phys. Rev. C **37**, 731-746 (1988)
- [37] T. Tomoda, Rep. Prog. Phys. **54**, 53-126 (1991).
- [38] F. Šimkovic, A. Faessler, H. Mütter, V. Rodin and M. Stauf, Phys. Rev. C **79**, 055501 (2009).
- [39] M. Horoi and S. Stoica, Phys. Rev. C **81**, 024321 (2010).
- [40] M. Kortelainen, O. Civitarese, J. Suhonen and J. Toivanen, Phys. Lett. B **647**, 128 (2007).
- [41] B.A. Brown and A.F. Lisetskiy (unpublished); See endnote (Ref. [28]) in B. Cheal et al. Phys. Rev. Lett. **104**, 252502 (2010).
- [42] R.A. Senkova and M. Horoi, Phys. Rev. C **90**, 051301 (2014).
- [43] R.A. Senkov, M. Horoi and B.A. Brown, Phys. Rev. C **89**, 054304 (2014).
- [44] D.L. Lincoln et al, Phys. Rev. Lett. **110**, 012501 (2013).
- [45] J. Menendez, A. Poves, E. Caurier and F. Nowacki, Phys. Rev. C **80**, 048501 (2009).
- [46] J. Barea and F. Iachello, Phys. Rev. C **79**, 044301 (2009).
- [47] ENSDF Data Base, Brookhaven National Laboratory, USA, <http://www.nndc.bnl.gov/ensdf/index.jsp>.
- [48] D. von Ehrenstein and J.P. Schiffer, Phys. Rev. **164**, 1374 (1967).
- [49] V.K.B. Kota and V. Potbhare, Nucl. Phys. **A331**, 93 (1979).
- [50] J.P. Schiffer et. al., Phys. Rev. Lett. **108**, 022501 (2012).
- [51] J.P. Schiffer *et al.* Phys. Rev. Lett. **100**, 112501 (2008).

- [52] B.P. Kay et. al. Phys. Rev. C **79**, 021301(R) (2009).
- [53] F. Boehm and P. Vogel, *Physics of Massive Neutrinos* (Cambridge University Press, Cambridge, 1992).
- [54] G. Audi, A.H. Wapstra and C. Thibault, Nucl. Phys. A **729**, 337 (2003).
- [55] A. Bobyk et al. Nucl. Phys. A **669**, 221 (2000)
- [56] J. Suhonen, Nucl. Phys. A **864** 63 (2011).
- [57] O. Civitarese and J. Suhonen, Nucl. Phys. A **653**, 321 (1999)
- [58] D.P. Ahalpara, K.H. Bhatt and R. Sahu, J. Phys. G **11**, 735 (1985)
- [59] S. Mishra, K.C. Tripathy and R. Sahu, Can. J. Phys. **85**, 269 (2007).
- [60] Caurier et al Phys. Lett. B **711**, 62 (2012)
- [61] L. Simard J. Phys. Conf. Ser. **375**, 042011 (2012).
- [62] P.A.R. Ade *et al.* (Planck collaboration), arXiv:1303.5076; Astronomy and Astrophysics **571**, A16 (2014).
- [63] P.S.B. Dev, S. Goswami, M. Mitra and W. Rodejohann, Phys. Rev. D **88**, 091301 (2013).
- [64] J. Menéndez, A. Poves, E. Caurier and P. Nowacki, Nucl. Phys. A **818**, 139 (2009).
- [65] V.A. Rodin, A. Faessler, F. Šimkovic, and P. Vogel, Nucl. Phys. A **793**, 213 (2007)
- [66] R. Sahu and V.K.B. Kota, arXiv:1501.07674 [nucl-th] 30 Jan 2015.

TABLE II: DSM results for half-lives for  $0\nu\beta\beta$  with  $m_\nu = 1$  eV (there are claims that the effective neutrino mass is certainly much less than 1 eV [62, 63]). The values of  $G^{0\nu}$  given in column 2 are taken from Ref. [53]. Columns 3 and 4 are DSM results. Fifth column gives current experimental bounds for the half lives. The last column gives the values of NTME predicted by other models along with the references. Note that in the table QRPA<sup>1)</sup> corresponds to calculations using QRPA with  $g_A = 1$  and QRPA<sup>2)</sup> corresponds to  $g_A = 1.25$ . See text for further details.

Nucleus	$G^{0\nu}(\text{yr}^{-1})$	$M^{0\nu}$	$T_{1/2}(\text{yr})$	$T_{1/2}(\text{yr})$	$M^{0\nu}$
		(DSM)	(DSM)	Expt'l bound (yr)	(other models)
<sup>70</sup> Zn	$0.23 \times 10^{-26}$	1.99	$1.1 \times 10^{26}$	$\geq 3.2 \times 10^{19}$	2.93 – 3.58 QRPA <sup>1)</sup> [56] 1.44 – 2.47 QRPA <sup>2)</sup> [56]
<sup>80</sup> Se	$0.43 \times 10^{-28}$	3.19	$2.3 \times 10^{27}$		
<sup>82</sup> Se	$0.11 \times 10^{-24}$	2.04	$2.2 \times 10^{24}$	$\geq 3.2 \times 10^{23}$	2.18 – 3.39 (SM) [4, 43, 64] 2.77 – 5.65 (QRPA) [7, 12, 38, 65] 4.41 – 4.84 (IBM-2) [8, 11, 46] 4.22 (GCM+PNAMP) [9]

TABLE III: DSM model predicted  $B(E2; J_i \rightarrow J_f)$  values in W.u. for  $^{80}\text{Kr}$  and  $^{82}\text{Kr}$  are compared with experimental data given in [47].

B(E2)'s for $^{80}\text{Kr}$				B(E2)'s for $^{82}\text{Kr}$			
$J_i$	$J_f$	DSM	Expt.	$J_i$	$J_f$	DSM	Expt.
$2^+$	$0^+$	23.1	$37.3 \pm 2.2$	$2^+$	$0^+$	17.8	$21.3 \pm 0.7$
$2'^+$	$2^+$	9.2	$25 \pm 5$	$2'^+$	$2^+$	8.4	$\approx 5.5$
$2'^+$	$0^+$	2.1	$0.30 \pm 0.07$	$2'^+$	$0^+$	2.6	
$4^+$	$2^+$	33.9	$70 \pm 10$	$3'^+$	$2^+$	4.6	
$3'^+$	$2'^+$	38.4	$34 \pm 5$	$3'^+$	$2'^+$	30.1	
$3'^+$	$2^+$	3.6	$0.57 \pm 0.14$	$4^+$	$2^+$	25.5	$32 \pm 12$
$4'^+$	$4^+$	7.2	$32 \pm 20$	$4'^+$	$2'^+$	6.0	$9 \pm 3$
$4'^+$	$2'^+$	11.0	$50 \pm 30$	$6^+$	$4^+$	27.9	$5.5 \pm 1.9$
$4'^+$	$2^+$	0.1	$0.26 \pm 0.18$	$5'^+$	$4^+$	0.3	$7.3 \pm 2.1$
$6^+$	$4^+$	38.8	$62 \pm 16$	$8^+$	$6^+$	27.4	
$5'^+$	$3'^+$	19.5	$50 \pm 17$	$10^+$	$8^+$	25.6	
$5'^+$	$4^+$	1.3	$1.2 \pm 0.7$				
$6'^+$	$6^+$	4.1	$17 \pm 15$				
$6'^+$	$4'^+$	20.2	$33 \pm 17$				
$6'^+$	$4^+$	0.1	$<0.23$				
$8^+$	$6^+$	38.7	$90^{+90}_{-45}$				
$10^+$	$8^+$	11.1					

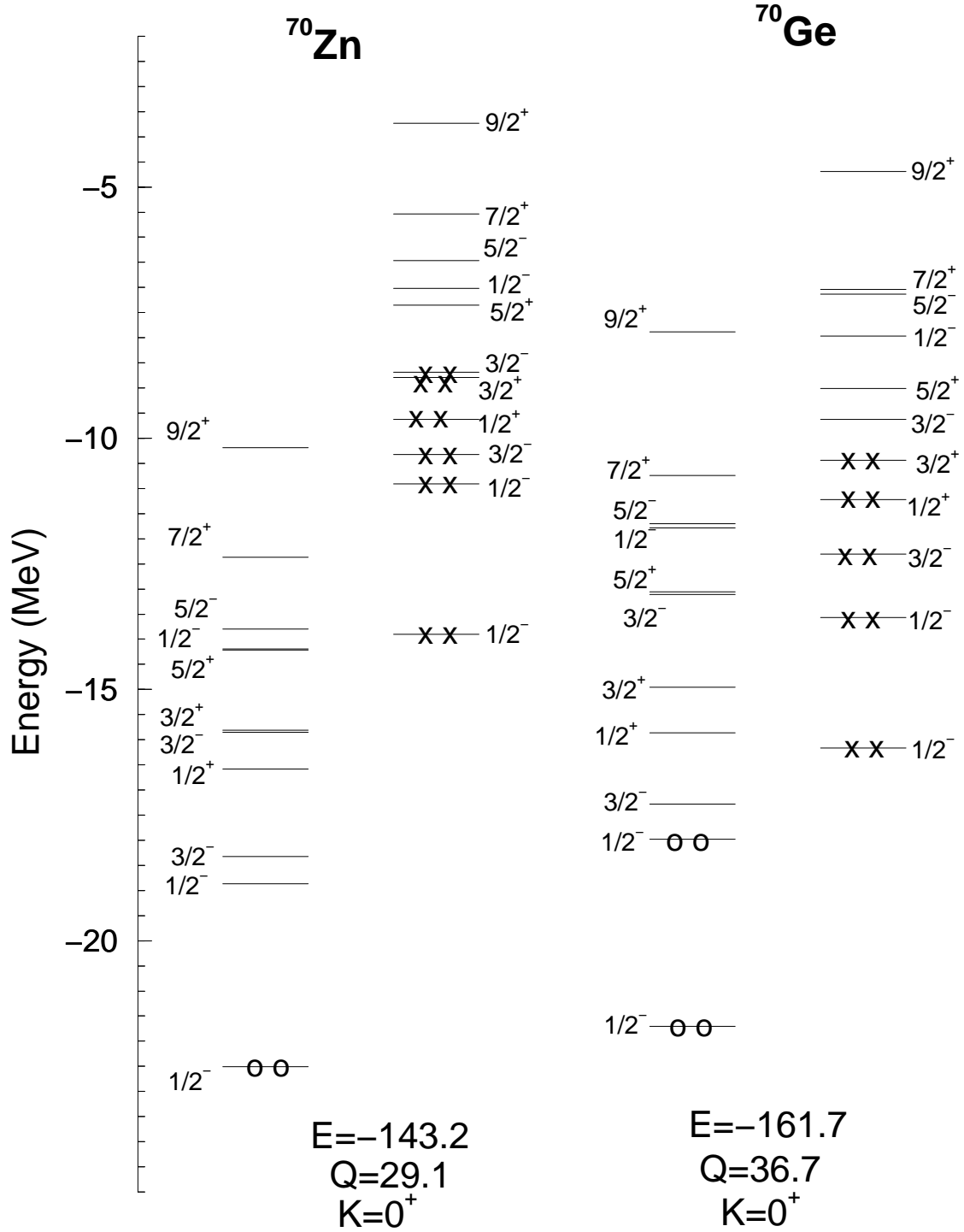


FIG. 1: HF single particle spectra for  $^{70}\text{Zn}$  and  $^{70}\text{Ge}$  corresponding to lowest prolate configurations. In the figures circles represent protons and crosses represent neutrons. The Hartree-Fock energy ( $E$ ) in MeV, mass quadrupole moment ( $Q$ ) in units of the square of the oscillator length parameter and the total  $K$  quantum number of the lowest intrinsic states are given in the figure. Each occupied single particle orbital is two fold degenerate because of time reversal symmetry.

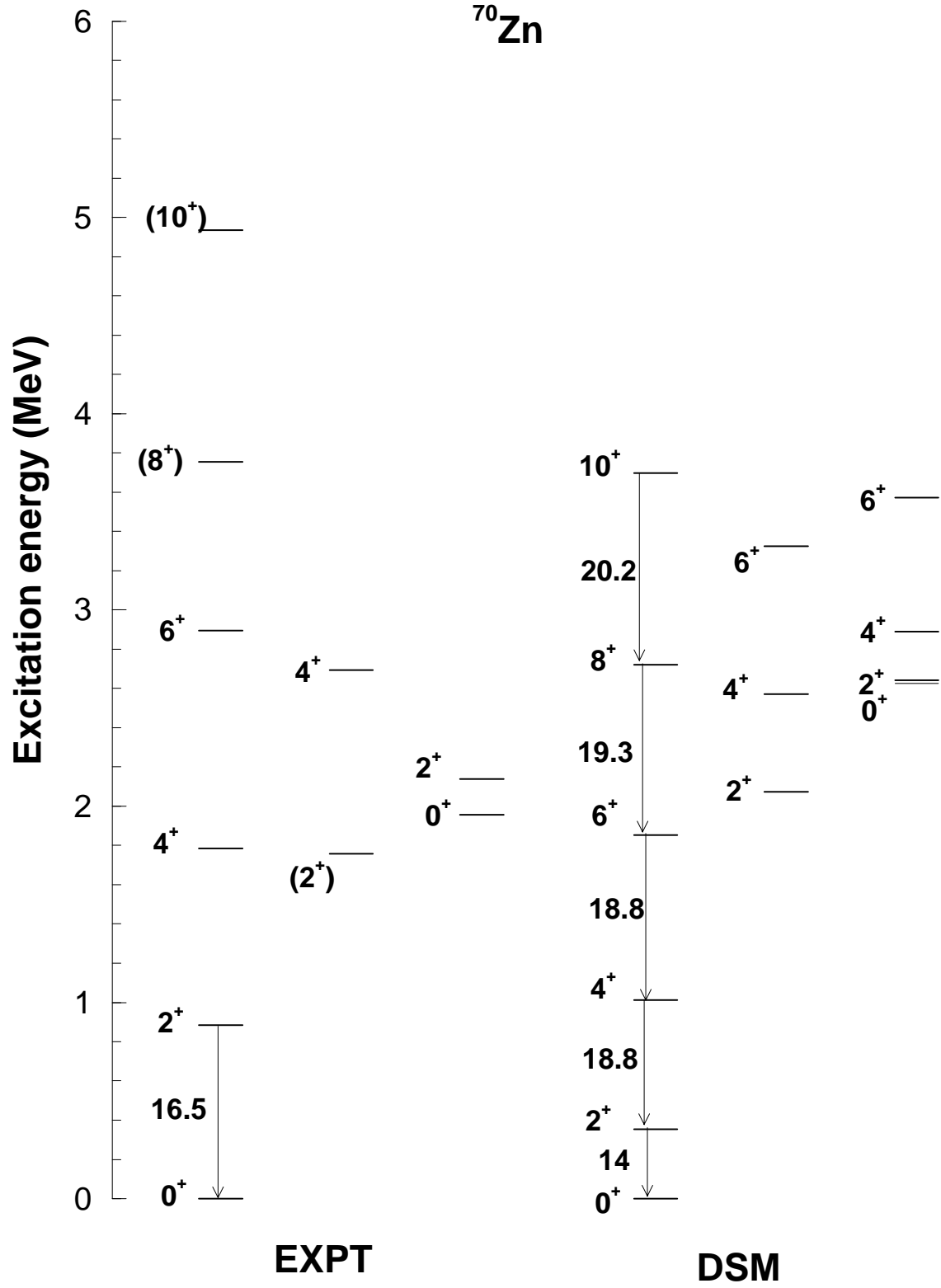


FIG. 2: The calculated energy levels for  $^{70}\text{Zn}$  are compared with experiment. The experimental data are from ref [47]. The quantities near the arrows represent  $B(E2)$  values in W.u.

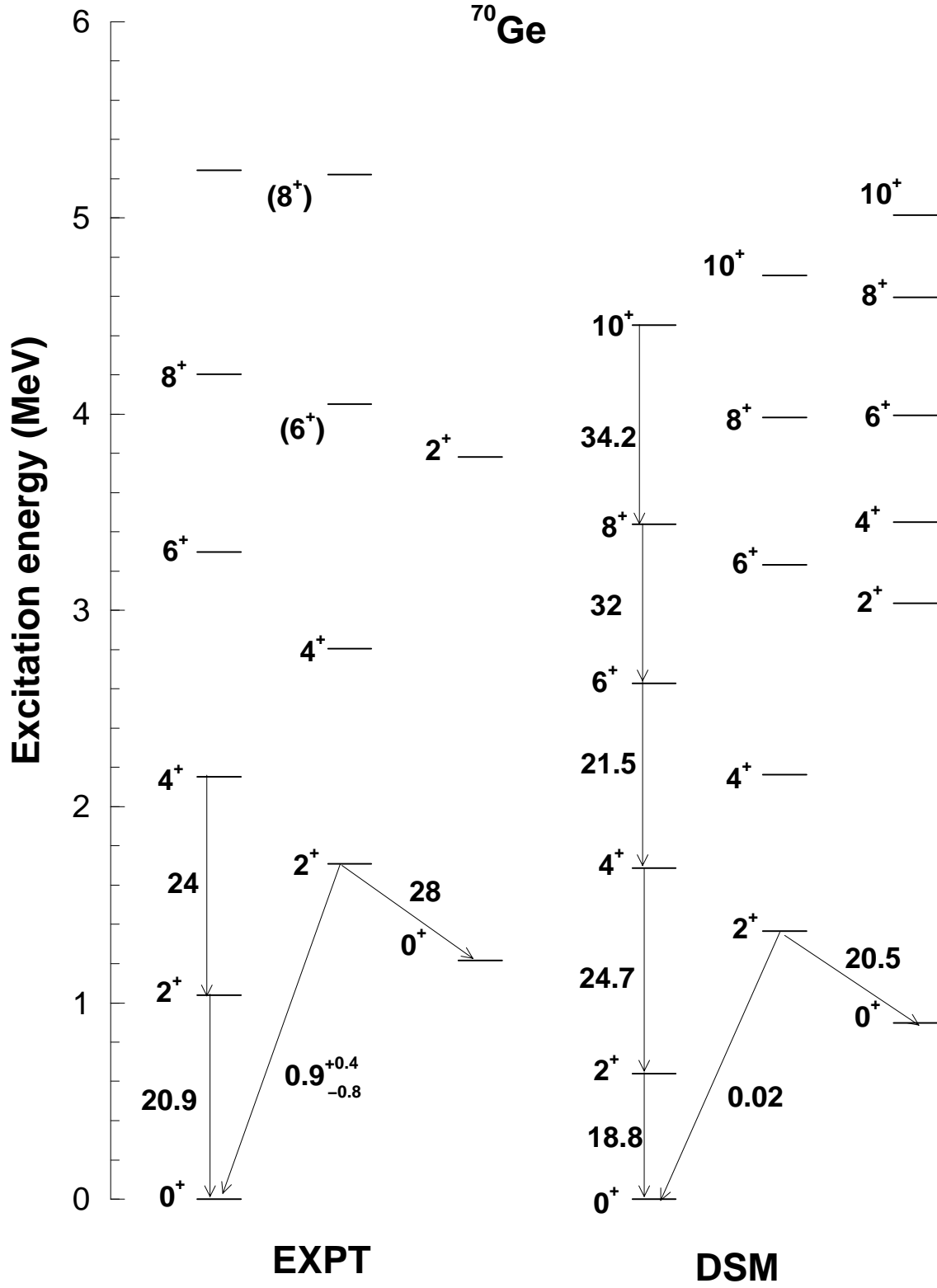


FIG. 3: The calculated energy levels for  $^{70}\text{Ge}$  are compared with experiment. The experimental data are from ref [47]. The quantities near the arrows represent  $B(E2)$  values in W.u.

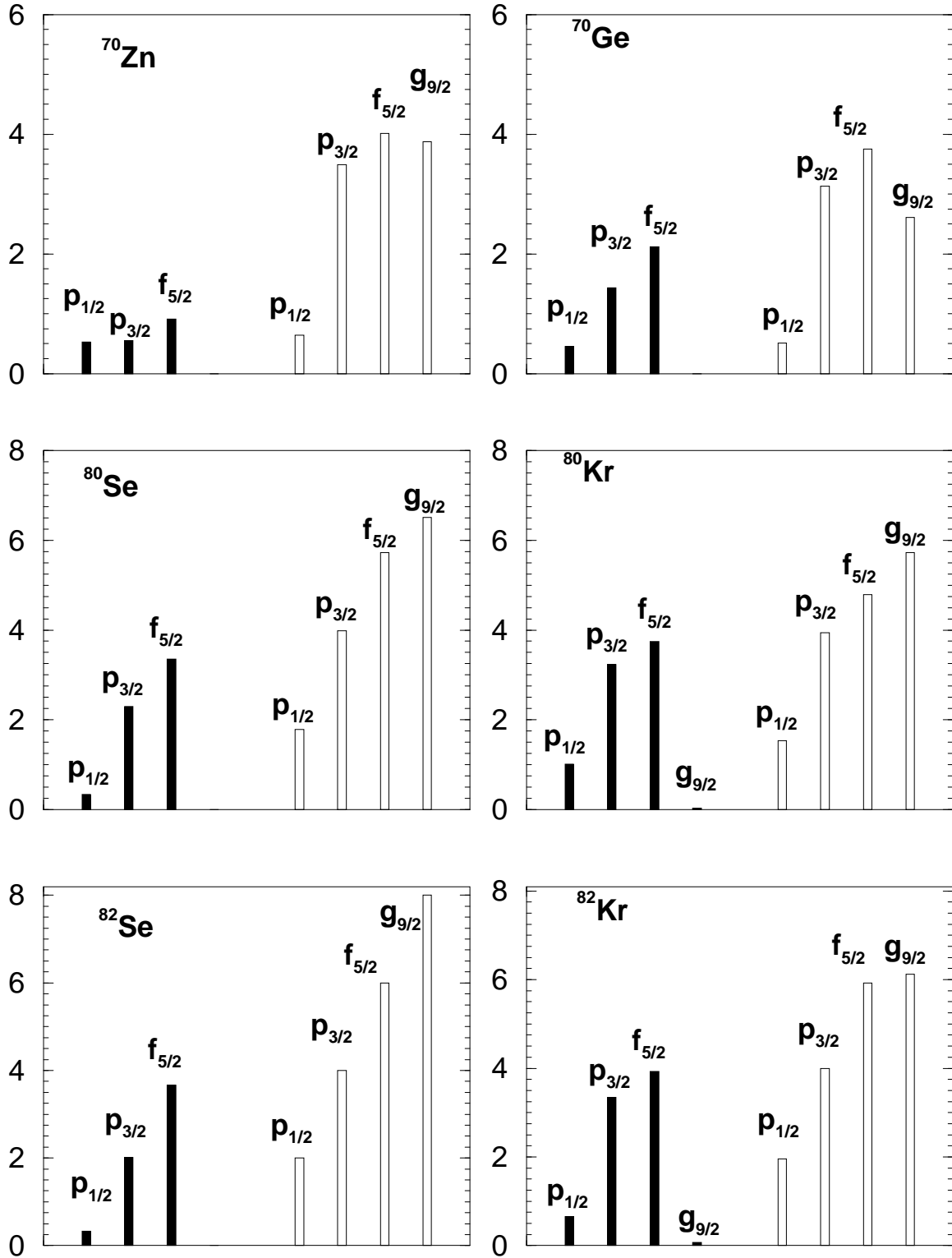


FIG. 4: DSM results for occupancies of different orbits. Filled bars are for proton occupancies and open bars are for neutron occupancies.



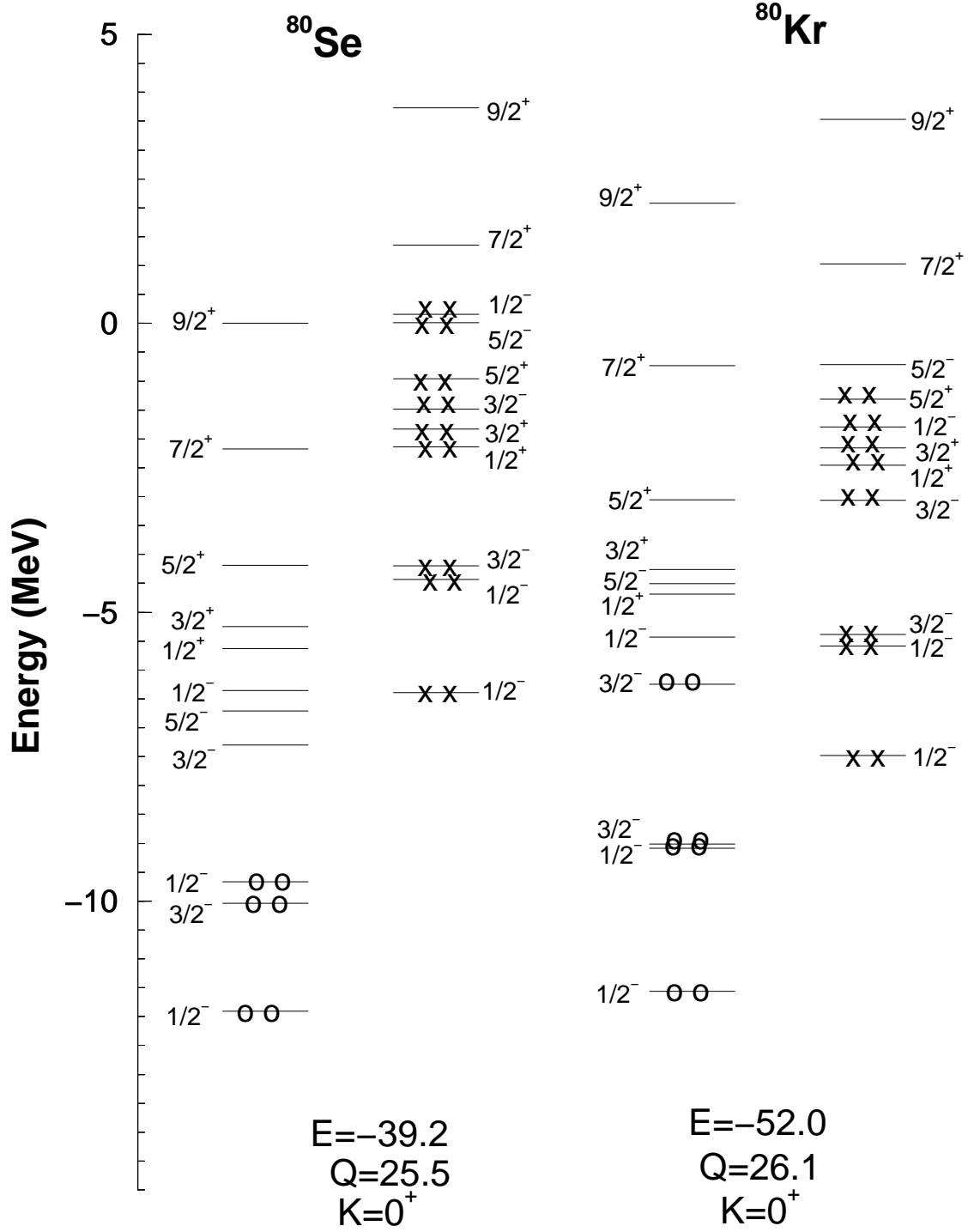


FIG. 5: HF single particle spectra for  $^{80}\text{Se}$  and  $^{80}\text{Kr}$  corresponding to lowest prolate configurations. In the figures circles represent protons and crosses represent neutrons. The Hartree-Fock energy ( $E$ ) in MeV, mass quadrupole moment ( $Q$ ) in units of the square of the oscillator length parameter and the total  $K$  quantum number of the lowest intrinsic states are given in the figure. Each occupied single particle orbital is two fold degenerate because of time reversal symmetry.

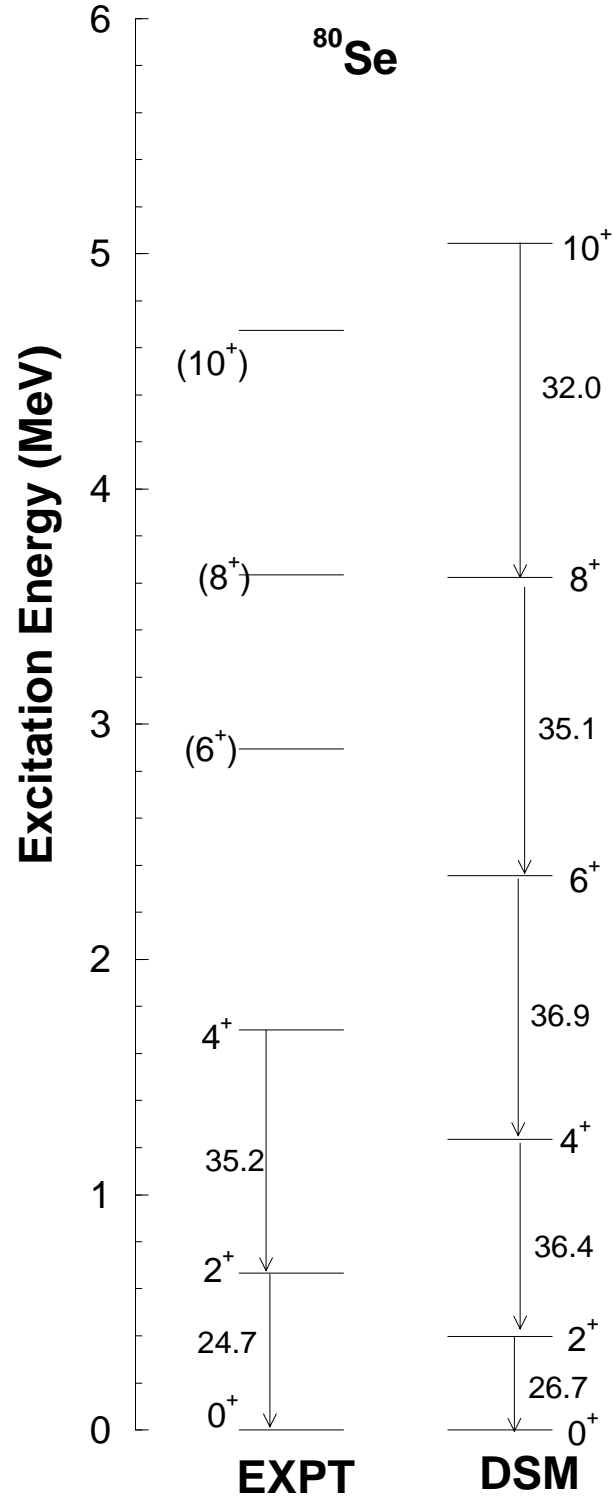


FIG. 6: The calculated energy levels for  $^{80}\text{Se}$  are compared with experiment. The experimental data are from ref [47]. The quantities near the arrows represent  $B(E2)$  values in W.u.

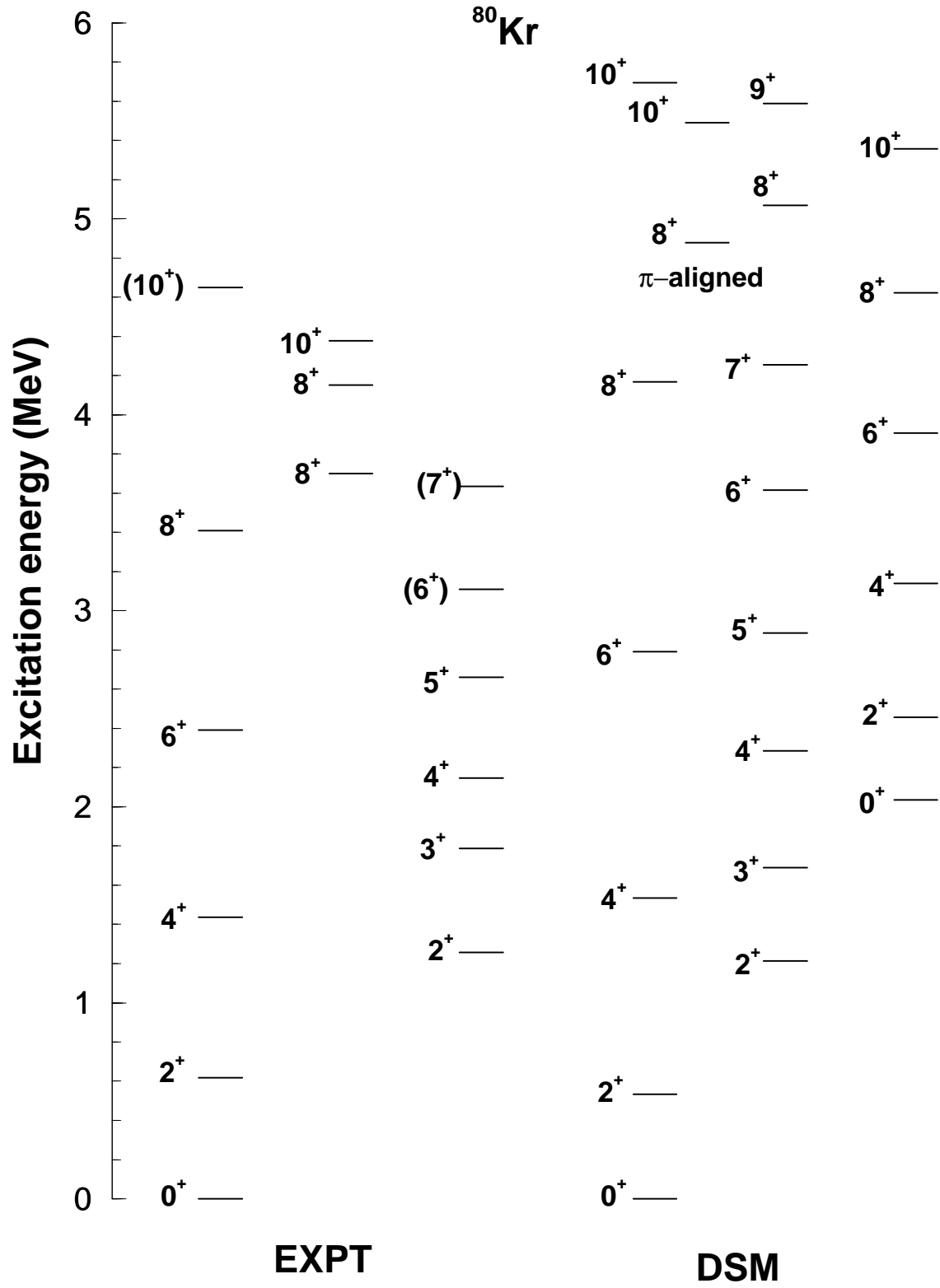


FIG. 7: The calculated energy levels for <sup>80</sup>Kr are compared with experiment. The experimental data are from ref [47].



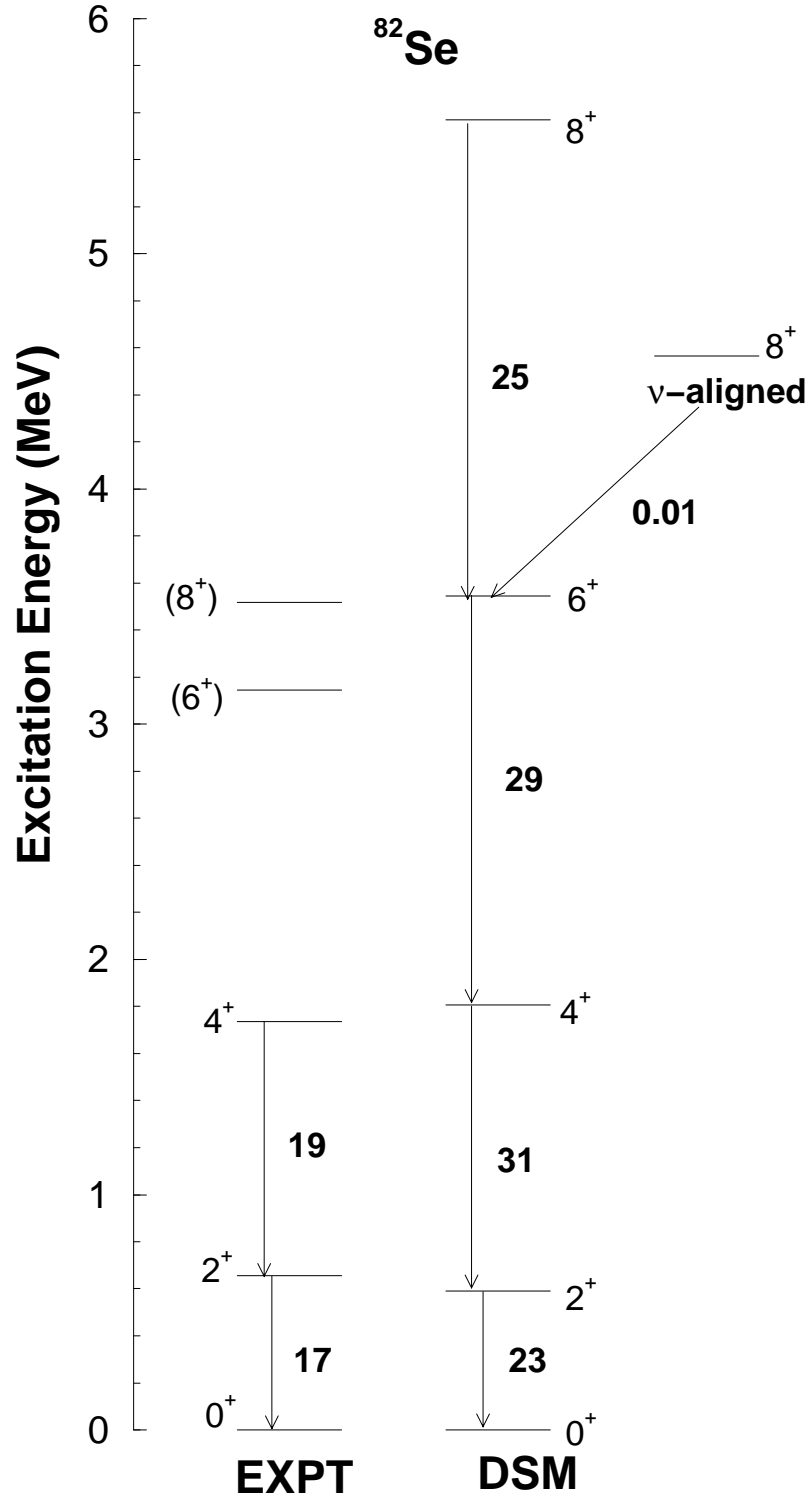


FIG. 9: The calculated energy levels for  $^{82}\text{Se}$  are compared with experiment. The experimental data are from ref [47].

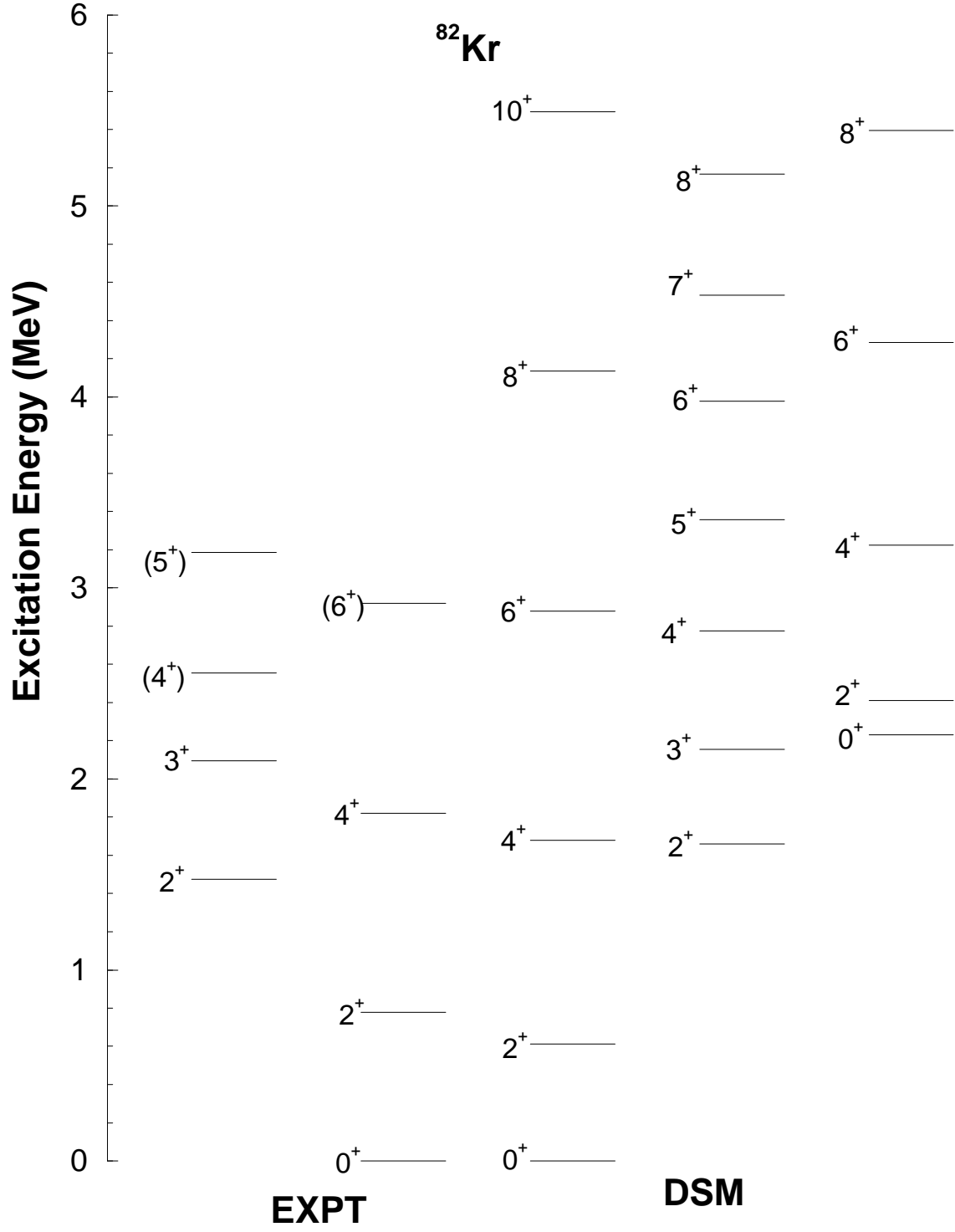


FIG. 10: The calculated energy levels for  $^{82}\text{Kr}$  are compared with experiment. The experimental data are from ref [47].